Neutron Spectra from Monoenergetic Photons on Bismuth*†

F. T. KUCHNIR,‡ P. AXEL, L. CRIEGEE,§ D. M. DRAKE, A. O. HANSON, AND D. C. SUTTON
Department of Physics, University of Illinois, Urbana, Illinois
(Received 19 April 1967)

Spectra of photoneutrons from a Bi^{209} target were obtained in the electric dipole giant-resonance region (12–16 MeV). A γ-ray energy resolution of 1.5% was attained using a bremsstrahlung monochromator; the neutron energies were measured with a time-of-flight technique with a resolution which varied from 10% at 2 MeV to 15% at 6 MeV. About 88% of the neutrons ejected by 14-MeV γ rays are statistical. The inferred level density of Bi^{208} near its ground state is not a simple function of excitation energy, but from 4 to 7 MeV it increases exponentially with energy; in that energy range the temperature is about 1 MeV. The nonstatistical high-energy neutrons leave the Bi^{208} nucleus at the excitation energies at which the states are well represented as single-neutron holes in Bi^{209}. These high-energy neutrons are intimately connected with the giant resonance. If the giant resonance is dominated by a single dipole state, the absolute width which characterizes the decay of the dipole state into the compound nucleus must increase by a factor of about 3 between 12 and 16 MeV.

I. INTRODUCTION

EARLY measurements of photoneutrons from bismuth indicated an excess of high-energy neutrons which had an angular distribution with a strong $\sin^2\theta$ component.[1] In addition, there was early evidence that these fast neutrons were connected with the giant dipole resonance.[2] A series of experiments on the energy and angular distribution of photoneutrons from bismuth[3–7] proved that γ rays produced mostly statistical neutrons, but that there were definitely some nonstatistical neutrons. However, these experiments, as well as many comparable ones on other nuclei, have left unsolved puzzles both about the statistical model for the compound nucleus which presumably governs the statistical neutrons, and about the giant resonance which plays a role in the emission of fast neutrons.

The present experiment[8] was designed to study photoneutron spectra obtained with good γ-ray resolution at neighboring γ-ray energies. The resulting data provide a decisive advantage over previous data because an essentially unambiguous separation can be made of statistical from nonstatistical neutrons. The analysis described in Sec. IV tests and confirms the statistical model, and determines some of its parameters. The fast neutrons give information about structure of the giant resonance and the dipole state. Before these results are presented, the experimental techniques will be described briefly in Sec. II. Section III covers the relevant features of the models being tested.

II. EXPERIMENTAL TECHNIQUE

A. Equipment

The University of Illinois bremsstrahlung monochromator[9,10] identifies photon energies by determining the energies of an electron before and after it emits a bremsstrahlung γ ray. The experimental arrangement is shown in Fig. 1. The incident electron is obtained from a 25-MeV betatron; the energy of the external electron beam is determined precisely by a bending magnet. The bremsstrahlung γ rays are produced in a thin converter which is placed at the source position of a second magnet which acts as a β-ray spectrometer.[11] The secondary electron is detected by a 3-in.-wide×1.62-in.-high×2-in.-thick pilot B plastic scintillator in the focal plane; the resulting pulse indicates both the energy of the corresponding photon and the time at which it was formed. Six electron detectors were used simultaneously to obtain data at six neighboring γ-ray energies. In the geometry used, the probability that the "tagged" γ ray would strike the target was measured to be about 0.27, 0.34, 0.40, and 0.46 for γ-ray energies of 10, 12, 14, and 16 MeV, respectively. (The probability was different for the different electron counters but was measured with a NaI scintillator whose efficiency was calculated.)

---

* This paper is based on the thesis submitted by F. T. Kuchnir in partial fulfillment of the requirements for a Ph.D. in Physics.

† Supported by the U. S. Office of Naval Research under Contract No. 1834 (05).

‡ Present address: Argonne National Laboratory, Argonne, Illinois.

§ Present address: DESY, Hamburg, Germany.

‖ Present address: Los Alamos Scientific Laboratory, Los Alamos, New Mexico.

[1] G. A. Price, Phys. Rev. **93**, 1279 (1954).

[2] F. Ferrero, A. O. Hanson, R. Malvano, and C. Tribuno, Nuovo Cimento 4, 418 (1956).

[3] G. N. Zatsepina, V. V. Igonin, L. E. Lazareva, and A. L. Lepestkin, Zh. Eksperim. i Teor. Fiz. 44, 1787 (1963) [English transl.: Soviet Phys.—JETP **17**, 1200 (1963)].

[4] Yu. Ya. Glazunov, M. V. Savin, I. N. Safina, E. F. Fomushkin, and Yu. A. Khoklov, Zh. Eksperim. i Teor. Fiz. **46**, 1906 (1964). [English transl.: Soviet Phys.—JETP **19**, 1284 (1964)].

[5] W. Bertozzi, P. T. Demos, S. Kowalski, F. R. Paolini, C. P. Sargent, and W. Turchinetz, Nucl. Instr. Methods **33**, 199 (1965).

[6] G. S. Mutchler, Ph.D. thesis, MIT, 1966 (unpublished).

[7] F. R. Allum, T. W. Quirk, and B. M. Spicer, Nucl. Phys. **53**, 545 (1964); see other references in this article.

[8] F. T. Kuchnir, University of Illinois, Ph.D. thesis, 1965 (unpublished); F. T. Kuchnir, P. Axel, L. Criegee, D. M. Drake, A. O. Hanson, and D. C. Sutton, Bull. Am. Phys. Soc. **10**, 542 (1965).

[9] J. S. O'Connell, P. A. Tipler, and P. Axel, Phys. Rev. **126**, 228 (1962).

[10] P. A. Tipler, P. Axel, N. Stein, and D. C. Sutton, Phys. Rev. **129**, 2096 (1963).

[11] J. S. O'Connell, Rev. Sci. Instr. **32**, 1314 (1961).

The energy of the photoneutrons was determined by a time-of-flight measurement made with an intrinsic time resolution of 2.5–3.0 nsec. The time-of-flight was measured with the aid of fast modular electronics. The maximum time-of-flight to which the system could respond was approximately 155 nsec, which would have been the flight time of 0.5-MeV neutrons. A time–to–pulse-height converter was used to obtain the input to a standard multichannel analyzer. (A 1024-channel Nuclear Data analyzer was divided into 8 separate 128-channel groups; the particular electron counter which was correlated with the neutron pulse provided the routing pulses.) In order to avoid an excessive number of chance coincidences, the primary electron beam was reduced to about 10^{-10} A. With the 4% duty cycle available, this beam current implied an average time separation of electrons in one electron detector of about 10 μsec during the beam. This low beam intensity made it necessary to reject very large pulses due to cosmic rays; without this special rejection, cosmic rays contributed to the apparent neutron background. A chance-coincidence spectrum was measured during each experimental run so that the data could be corrected for chance coincidences. This correction was simplified by the availability in each spectrum of obvious backgrounds at times corresponding to both higher-energy neutrons than were energetically possible and lower-energy neutrons than could activate the detector system.

The neutron detector consisted of a cylindrical Pyrex container, 6 in. in diameter and 3 in. deep, which was filled with NE 213 liquid scintillator.[12] An Amperex 58 AVP and an RCA 6810A phototube, both biased well into noise, were used in coincidence in order to view this scintillator without recording too many noise pulses. Space-charge saturation at the 58 AVP anode[13] was used

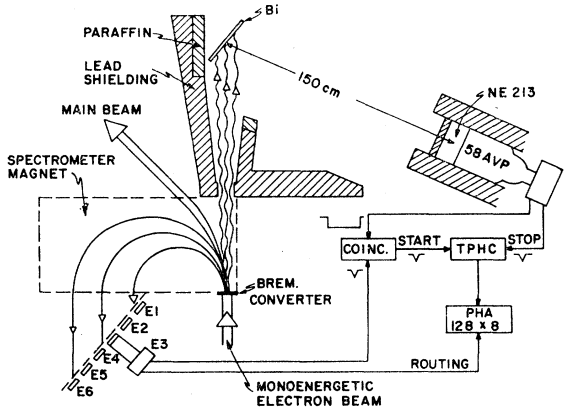

FIG. 1. Schematic diagram of the experimental arrangement. The monoenergetic electron beam is extracted from a 25-MeV betatron and its energy is determined by a bending magnet.

[12] Purchased from Nuclear Enterprises, Ltd., Winnipeg, Manitoba, Canada.

[13] R. B. Owen, Nucleonics 17, No. 9, 92 (1959).

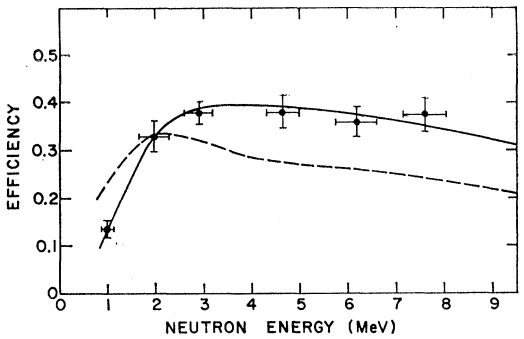

FIG. 2. Efficiency of the neutron detector. The solid line, drawn through the experimental points to guide the eye, represents the efficiency actually used in the preliminary analysis of the data. The dashed line is the effective efficiency appropriate to the data taken at 14 MeV; it includes a correction for resolution and line shape. Each experimental point was obtained with a monochromatic photon beam of the appropriate energy.

to discriminate against the prohibitively high γ-ray background. The neutron detector was placed at 150 cm from the $\frac{3}{8}$-in.-thick Bi^{209} target. The normal to the sample made an angle of 50° with respect to the incoming beam; the neutron detector was at 115° and its front face was therefore not quite parallel to the sample.

The calibration of the neutron-detector efficiency was made by using a deuterium target as a standard. An attempt was also made to calculate the expected efficiency using a Monte Carlo program. However, the experimental arrangement was too complex to permit a detailed calculation. Some of the complicating factors are listed below: (1) Because of very low counting rates, the detector was moved to 50 cm from the D_2O target. (2) Corrections were required for the scattering of the monoenergetic neutrons in the D_2O target. (3) The neutron detector was shielded from γ rays by 1-in. Pb on the front face and 3-in. Pb around it. (4) The effect on small voltage pulses of the circuit discriminating γ rays from neutrons was not well known.

The experimental points in Fig. 2, with the solid line to guide the eye, show the measured efficiency as a function of neutron energies after corrections were made for neutron scattering in the deuterium sample. The measured time distribution of the pulses corresponding to monoenergetic neutrons after correcting for scattering in the deuterium target was a skewed Gaussian with a small tail at long times; these late pulses are interpreted as due to neutrons arriving late because of scattering in the detector's Pb shield and in other material around the room. Thus, it was necessary to introduce a line-shape correction which gave the probability that a neutron which leaves the sample with energy E_n is detected at a time corresponding to an energy E_n'. The combined effect of this line-shape correction and the resolution were included in a probability function $R(E_n,E_n')$.

For the apparent neutron spectrum detected, $dN' \times(E_n',E_\gamma)/dE_n'$ can be expressed in terms of the

"true" neutron spectrum $dN(E_n,E_\gamma)/dE_n$ by using the efficiency $\epsilon(E_n)$ and the resolution probability function:

$$\frac{dN'(E_n',E_\gamma)}{dE_n'}=\int_0^{E_{n\,\max}}\frac{dN(E_n,E_\gamma)}{dE_n}\epsilon(E_n)\times R(E_n,E_n')dE_n. \quad (1)$$

If the resolution were very good [i.e., if $R(E_n,E_n')$ could be approximated by a δ function], the true spectrum could be expressed simply in terms of the observed spectrum as

$$\frac{dN(E_n,E_\gamma)}{dE_n}\simeq\frac{1}{\epsilon(E_n)}\frac{dN'(E_n,E_\gamma)}{dE_n}. \quad (2)$$

A correction for resolution and line shape could be made by using different effective neutron efficiencies at different γ-ray energies. The qualitative effect of the resolution function on the neutron efficiency is clear. Scattered high-energy neutrons give a late signal corresponding to a lower energy; this can be taken care of by using an effective efficiency which is lower than the measured efficiency for high-energy neutrons. In a similar way, a correction is needed for low neutron energy, because some of the neutrons which appear to have low energy are actually due to the "late" higher-energy neutrons. This correction would correspond to an increase in effective efficiency in the low-energy region. Because the tails due to the different high-energy neutrons add up, the effective efficiency for low neutron energy is considerably greater than the solid line shown in Fig. 2.

The dashed curve in Fig. 2 illustrates the effective efficiency appropriate to the data obtained with 14-MeV γ rays. This efficiency should, in principle, include the inelastic scattering of neutrons in the Bi^{209} sample.

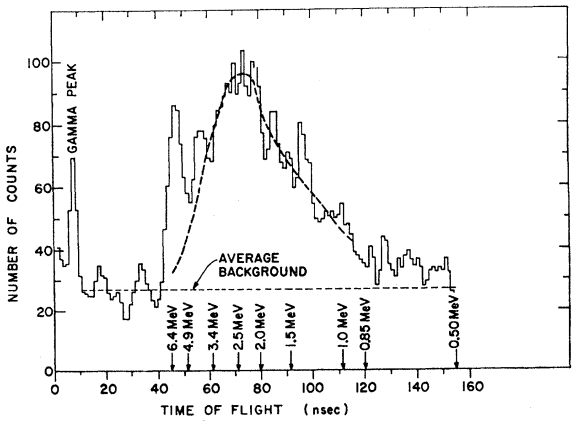

FIG. 3. Typical neutron time-of-flight spectrum from the $Bi^{209}(\gamma,n)$ reaction obtained at $E_\gamma=13.85\pm0.15$ MeV and a flight path of 150 cm. Data shown are as obtained from the time-to-pulse-height converter; no correction for detector efficiency has been applied. The dashed line is a typical evaporation spectrum as described in the text. The γ peak was used as a time reference.

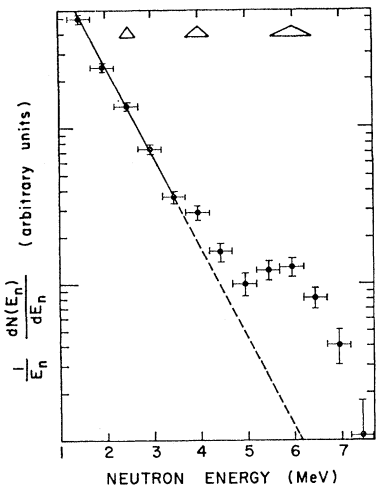

FIG. 4. Semilogarithmic plot of the spectrum resulting from the data shown in Fig. 3 after dividing by the neutron energy and correcting for the detector efficiency (solid line in Fig. 2). Triangles represent the neutron-energy resolution. The solid line extrapolated to higher neutron energies is the result of a least-squares fit to the five lowest-energy points. The apparent nuclear temperature represents only a lower limit since the line-shape correction has not been included.

However, because the sample thickness was only 0.0178 atoms/b in the direction of the neutron detector, this correction was small compared with the line-shape correction and was neglected. Some of the analysis was carried out using the uncorrected efficiency represented by the solid line in Fig. 2. Those parts of the analysis which were sensitive to the effective efficiency correction were also carried out using the function represented by the dotted line in Fig. 2 which will be called effective neutron efficiency.

B. Typical Data and Data Reduction

The time-of-flight data obtained at 150-cm flight path for 13.85-MeV γ rays (very near the peak of the giant resonance) are shown in Fig. 3. The average background, which consists mainly of chance coincidences, is shown. The apparent excess of counts beyond 130 nsec is interpreted as due mainly to neutrons scattered off the lead shielding. The data in Fig. 3 were obtained during 100-h beam time. Spectra obtained at other energies are similar, although sometimes slightly inferior in statistics and neutron resolution.

The dashed curve in Fig. 3 is included to illustrate the shape of an evaporation spectrum. This curve is based on a constant nuclear temperature of 0.8 MeV and the uncorrected efficiency represented by the solid line in Fig. 2. A very similar curve would be obtained with a corrected efficiency function and a nuclear temperature of about 1 MeV. This figure illustrates clearly the excess of high-energy neutrons (near 50 nsec). The γ-ray peak, in the time region below 10 nsec, was used as a convenient time reference. For this purpose, the

circuit which discriminated against γ rays was adjusted to allow a few γ rays to be recorded.

The 13.85-MeV γ-ray data are also presented in a more conventional form in Fig. 4, which shows the logarithm of $(1/E_n)dN(E_n)/dE_n$ plotted as a function of the neutron energy E_n. The uncorrected neutron efficiency was applied to the data. The line, which is the result of a least-squares fit to the five lowest-energy points, corresponds to the same theoretical evaporation spectrum shown by the dotted line in Fig. 3. The neutron-energy resolutions are shown by the triangles. The vertical extensions of the experimental points represent only the statistical errors. The horizontal extensions show the energy intervals into which the experimental data were grouped.

The measurements made at all γ-ray energies can be analyzed together because the energy dependence of the photon-absorption cross section is well known.[14,15] The data were reduced to a form which made this analysis possible by dividing the number of observed neutrons $dN(E_n,E_\gamma)$ by a factor proportional to the number of absorbed γ rays given by the product of the measured number of incident γ rays N_γ and the nuclear absorption $\sigma_a(E_\gamma)$ taken from Ref. 15. The resulting number is proportional to the probability $dP(E_n,E_\gamma)$ that an interacting photon of energy E_γ will produce a neutron in the energy range between E_n and E_n+dE_n:

$$\frac{dP(E_n,E_\gamma)}{dE_n}=\frac{1}{cN_\gamma\sigma_a(E_\gamma)}\frac{dN(E_n,E_\gamma)}{dE_n}, \tag{3}$$

where c represents the proportionality factor.

It is convenient for the analysis of the data to express $dP(E_n,E_\gamma)$ in terms of the excitation energy U in the residual nucleus:

$$U=E_\gamma-E_n-E_B, \tag{4}$$

where E_B is the neutron binding energy which is 7.43 MeV for bismuth. We also define a discrete probability function as

$$\Delta_jP(U_j,E_\gamma)=\int_{U_j-\delta/2}^{U_j+\delta/2}dP(U,E_\gamma). \tag{5}$$

Equation (5) uses the obvious notation for $dP(U,E_\gamma)$ in place of $dP(E_n,E_\gamma)$; δ is the width of the equal-energy intervals into which the experimental data were grouped. The interval index j, and the residual excitation U_j fall between the following limits:

$$1\leq j\leq j_{\max},\quad j_{\max}=(1/\delta)(E_\gamma-E_B), \tag{6}$$

$$(j-1)\delta\leq U_j\leq j\delta. \tag{7}$$

All of the neutron measurements at different γ-ray energies were reduced to $\Delta_jP(U_j,E_\gamma)$ for the allowed intervals j.

III. THEORETICAL GUIDANCE FOR DATA ANALYSIS

Because of the evidence for the existence of two main components in the photoneutron spectra, Δ_jP is expressed as the sum of Δ_jP_S and Δ_jP_D corresponding to the statistical and nonstatistical processes, respectively:

$$\Delta_jP(U_j,E_\gamma)=f_S(E_\gamma)\Delta_jP_S(U_j,E_\gamma)+[1-f_S(E_\gamma)]\Delta_jP_D(U_j,E_\gamma). \tag{8}$$

$f_S(E_\gamma)$ is the fraction of neutrons emitted in the statistical process at an energy E_γ. All of the 120 data were fitted simultaneously using Eq. (8); the following sections indicate the nuclear models that were used to select the very few appropriate parameters which were allowed to vary.

A. Statistical Neutrons

In the statistical model, the differential probability $dP_S(U,E_\gamma)$, is the product of the level density $\rho(U)$ and a kinematic factor $K(E_n)$ which depends on the energy of the neutron:

$$dP_S(E_n,U)\propto K(E_n)\rho(U)dU. \tag{9}$$

In the analysis of experimental data related to the statistical model, several expressions for $\rho(U)$ have been used. Popular forms include

$$\rho=\rho_0e^{U/T}, \tag{10a}$$

$$\rho=\rho_0\exp[2(aU)^{1/2}], \tag{10b}$$

$$\rho=\rho_0\frac{\exp[2(a'U)^{1/2}]}{U^2}. \tag{10c}$$

The present experiment provides enough data to determine the sum of levels in different energy intervals without imposing a preselected functional form for $\rho(U)$. If we call $\Delta_i\rho(U_i)$ this sum for the ith interval, it can be defined as

$$\Delta_i\rho(U_i)\equiv\frac{1}{K(E_{ni})}\int_{U_i-\delta/2}^{U_i+\delta/2}dP_S(E_n,U)dU. \tag{11}$$

The probability $\Delta_iP_S(U_i,E_\gamma)$ that the compound nucleus will decay to the ith interval in the residual nucleus is

$$\Delta_iP_S(U_i,E_\gamma)=K(E_{ni})\Delta_i\rho(U_i)/\sum_{j=1}^{j_{\max}}K(E_{nj})\Delta_j\rho(U_j). \tag{12}$$

Equation (12) when applied to the same ith interval

[14] B. M. Spicer, Nuovo Cimento Suppl. 2, 243 (1964).
[15] R. R. Harvey, J. T. Caldwell, R. L. Bramblett, and S. C. Fultz, Phys. Rev. 136, B126 (1964).

for two different γ-ray energies, $E_{\gamma 1}$ and $E_{\gamma 2}$, yields

$$\frac{\Delta_i P_S(U_i,E_{\gamma 2})/K(E_{ni_2}) \sum_{j=1}^{j\max 1} K(E_{nj_1})\Delta_j\sigma(U_j)}{\Delta_i P_S(U_i,E_{\gamma 1})/K(E_{ni_1}) \sum_{j=1}^{j\max 2} K(E_{nj_2})\Delta_j\rho(U_j)}. \quad (13)$$

The numerator and denominator on the right side of Eq. (13) are only functions of $E_{\gamma 1}$ and $E_{\gamma 2}$, respectively. Therefore, for $E_{\gamma 2}>E_{\gamma 1}$, the right-hand side of Eq. (13) represents a decrease which has exactly the same effect on all intervals i when data for $E_{\gamma 2}$ are compared to data for $E_{\gamma 1}$. This decrease provides a signature for compound nuclear events, and indeed forms an unambiguous phenomenological basis for the definition of statistical decay. This makes it possible to determine an energy-level density at low excitation energy despite the relatively small number of statistical events reaching low excitation energy. It also makes possible a more reliable separation of statistical and nonstatistical neutrons than had been possible in earlier experiments.

As long as the first term on the right-hand side of Eq. (8) dominates, the experimental points will follow a pattern characteristic of the statistical decay with the properties described by Eqs. (12) and (13). In order to display these properties more clearly it was found convenient to divide the experimental quantities defined by Eqs. (3)–(5), $\Delta_j P(U_j,E_\gamma)$, by a kinematic factor $K(E_{nj})$. Figure 5 shows the result when the neutron energy E_{nj} is used as an approximate kinematic factor. All of the points corresponding to a particular interval i are given the same symbol. For example, filled circles are used for $U_i=4.5$ MeV, open circles for $U_i=3.5$ MeV, etc. The values of U_i are indicated and the dashed lines represent least-squares fits to the data as will be described below. Each set of points which appear on a vertical line represents a single time-of-flight spectrum obtained at one γ-ray energy such as is illustrated in Figs. 3 and 4. The data include all of the experimental points obtained at a flight path of 150 cm and were collected over a period of 3 weeks of 24 h/day running time.

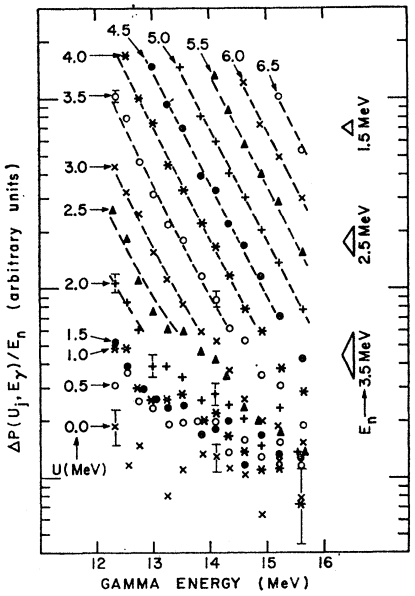

FIG. 5. The quantity $\Delta P_j(U_j,E_\gamma)/E_n$ as defined by Eqs. (3)–(5) is plotted for all experimental data. Each set of points which appear on a vertical line represents a single time-of-flight spectrum such as is illustrated in Figs. 3 and 4. The efficiency function represented by the solid line in Fig. 2 was used in the data reduction. The parallel lines, characteristic of compound nuclear processes, are the partial result of the least-squares fit of Eq. (8) to all 120 points in the figure. The vertical neutron-energy scale on the right applies only for the points which follow the straight-line pattern. The existence of nonstatistical neutron emission results in the breakdown of the parallel-line pattern. This form of presenting the data illustrates the strong internal consistency restrictions imposed by the present analysis in the separation of statistical from nonstatistical neutrons. (The data presented here were not corrected for effective efficiency.)

The upper portion of Fig. 5 provides an excellent illustration of the pattern expected for compound nuclear processes. If only compound nuclear processes occurred, the curves connecting points corresponding to a given interval i should be parallel and should decrease with γ-ray energy due to the competition factor in Eq. (13). Their slopes with respect to E_γ should be intimately connected to the variation of level density with U, $d\rho(U)/dU$, at excitation energies near the newly opening channels. The spacing between the lines corresponding to intervals $i+1$ and i at any γ-ray energy should depend only on the factor $\Delta_{i+1}\rho(U_{i+1})/\Delta_i\rho(U_i)$. [The curves would be straight lines on this semilogarithmic plot if $\rho(U)\propto\exp(U/T)$, where T is constant. The straight-line pattern has the advantage that while it persists, horizontal lines correspond to lines of constant neutron energy. Typical neutron energies and resolutions are shown on the right of Fig. 5.] The same data, corrected for the effective efficiency are shown in Fig. 6, which displays the same pattern for the statistical process. No correction was needed for the $(\gamma,2n)$ process even though its threshold is about 14.3 MeV because none of the neutrons represented in Figs. 5 or 6 has low enough energy to be attributable to the decay of Bi^{208}.

B. Nonstatistical Neutrons from the Giant Dipole Resonance

Although this statistical pattern of equally spaced lines fits the data in the upper portion of Fig. 5 reasonably well, there are undoubtedly excess neutrons which leave the residual nucleus at excitation energies of 2 MeV and below. One obvious source of these nonstatistical neutrons is the particle-hole dipole state[16,17]

[16] D. H. Wilkinson, Physica **22**, 1039 (1956); See also Ann. Rev. Nucl. Sci. **9**, 1 (1959).

[17] G. E. Brown and M. Bolsterli, Phys. Rev. Letters **3**, 472 (1959).

formed when a photon excites a nucleon from one occupied orbit (thereby creating a "hole") to an unoccupied orbit (in which it is called the "particle"). The simplest model which has been suggested to explain the emission of nonstatistical neutrons treats the complicated giant resonance as though it were a simple resonance[16,18] associated with a single dipole state. The resonance is characterized by a partial width Γ_D for neutron emission from the dipole state, and a width Γ_C for the decay of the dipole state into the more complicated configurations which lead to the compound nucleus and its statistical decay. (A partial width for photon emission is also present, but it is only about 40 keV and can be neglected in our analysis.) The following paragraphs will summarize the theoretical guidance available for the simple particle-hole wave function of the dipole state, the direct neutron emission from it, and the competition between neutron emission and compound-nucleus formation.

Both the early single-particle model of Wilkinson[16] and the schematic model of Brown and Bolsterli[17] make it clear that the most important particle-hole configurations in the dipole state are those in which the particle quantum numbers l_p, j_p are related simply to the hole quantum numbers l_h, j_h:

$$l_p=l_h+1, \quad j_p=j_h+1. \tag{14}$$

The more realistic calculations performed[19–22] for Pb^{208} confirm the dominance of these configurations. The first[19] used harmonic-oscillator wave functions, experimental energies for the particle and hole states, and a δ-function residual interaction with an exchange mixture. Pal, Soper, and Stamp[20] improved this calculation by using Saxon-Woods wave functions, and more (i.e., 31) particle-hole states. They later[21] increased the number of particle-hole states to 35, and it is this calculation which is used in the analysis of our data. The above calculations gave approximately the correct energy for the giant dipole resonance, and indicated that the strength was concentrated in one state and a single weaker, neighboring satellite. The energies and percentages of the dipole strength associated with these strong states in the three calculations are: 13.8 MeV (58%) and 13 MeV (18%),[19] 13.4 MeV (54%), and 12.6 MeV (37%),[20] and 12.9 MeV (72%), and 13.6 MeV (16%).[21] The relatively small spacing between these states compared to the 3.8-MeV width observed

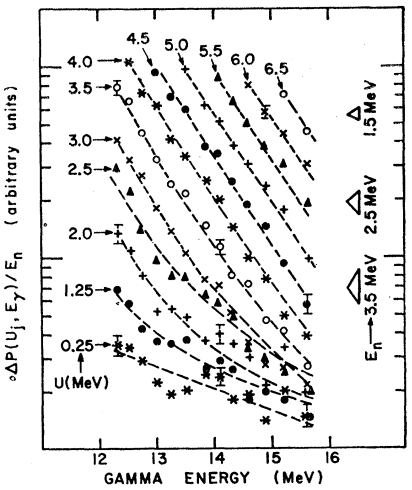

FIG. 6. The same data of Fig. 5 are plotted after applying a correction for the effective efficiency, as shown in Fig. 2. The data of the lowest four 0.5-MeV intervals of Fig. 5 are combined into 1-MeV intervals due to poor statistics and energy resolution and also for clarity of display. The lines are the result of a least squares fit of Eq. (8) as is described in the text.

for the giant resonance suggests the simplifying assumption that the entire giant resonance is dominated by a single dipole state. Table I gives the squared amplitudes of the particle-hole components of this dipole state for the calculation of Ref. 21. (The intensities used are a

TABLE I. Squared amplitudes $\mathfrak{a}$ for the neutron particle-hole configurations in the giant dipole state of Pb^{208}. These amplitudes are a weighted sum of the squared amplitudes of the strongest dipole state and its weak satellite as given in Ref. 21. The neutron penetrabilities were computed for a square well of $R=1.41A^{1/3}$ F.

Excitation energy of hole in Bi^{208} (MeV)	Configuration Hole	Particle	$100\mathfrak{a}^2$	Neutron penetrabilities $E_\gamma=12$ MeV	$E_\gamma=14$ MeV	$E_\gamma=16$ MeV
0.0	$p_{1/2}$	$s_{1/2}$	0.0062	3.9	4.7	5.4
		$d_{3/2}$	0.181	3.2	4.1	4.8
0.57	$f_{5/2}$	$d_{3/2}$	0.012	2.8	3.8	4.6
		$d_{5/2}$	0.0033	2.8	3.8	4.6
		$g_{7/2}$	2.56	1.0	2.1	3.1
0.9	$p_{3/2}$	$s_{1/2}$	0.0049	3.5	4.4	5.1
		$d_{3/2}$	0.031	2.7	3.7	4.5
		$d_{5/2}$	0.490	2.7	3.7	4.5
1.6	$i_{13/2}$	$h_{11/2}$	0.663	0.11	0.67	1.6
		$j_{13/2}$	3.79	0.00	0.02	0.15
		$j_{15/2}$	13.0	0.00	0.02	0.15
2.3	$f_{7/2}$	$d_{5/2}$	0.0067	1.7	3.0	3.9
		$g_{7/2}$	0.090	0.24	1.2	2.3
		$g_{9/2}$	3.14	0.24	1.2	2.3
3.5	$h_{9/2}$	$g_{7/2}$	0.72	0.03	0.65	1.7
		$g_{9/2}$	0.017	0.03	0.65	1.7
		$i_{11/2}$	10.6	0.00	0.02	0.19
6.9	$h_{11/2}$	$g_{9/2}$	0.39	0.00	0.00	0.10
		$i_{11/2}$	0.91	0.00	0.00	0.00

[18] G. E. Brown and J. S. Levinger, Proc. Phys. Soc. (London) A71, 733 (1958).
[19] V. V. Balashov, V. G. Shevchenko, and N. P. Yudin, Zh. Eksperim. i Teor. Fiz. 41, 1929 (1961) [English transl.: Soviet Phys.—JETP 14, 1371 (1962)].
[20] M. K. Pal, J. M. Soper, and A. P. Stamp, Atomic Energy Research Establishment, Harwell, Report T.P. 148, 1964 (unpublished); also work to be published.
[21] These data and considerable additional useful information about these calculations were made available by Dr. J. M. Soper.
[22] V. Gillet, A. M. Green, and E. A. Sanderson, Nucl. Phys. 88, 321 (1966).

weighted average of the squared amplitudes of the two states mentioned above.) These amplitudes will be used for Bi^{209}, whose giant resonance is very similar[23] to that of Pb^{208}. (This corresponds to assuming that the extra proton in Bi^{209} has a negligible effect on the giant resonance.)

Despite the semiquantitative agreement mentioned above, there is not unanimity about the number of strong dipole states in the giant-resonance region. Gillet, Sanderson, and Green[22] have calculated the energies and wave functions of single particle-hole states of different spin and parity in Pb^{208}. They used a finite-range residual interaction with a range determined from two-nucleon scattering and with a strength and exchange mixture based on calculations of levels in light nuclei. Although they obtained reasonable agreement with experiment for some of the levels with different spin and parity, their results are not in good agreement with the giant dipole resonance. Gillet *et al.* do find a strong state with almost 60% of the dipole strength but it has an energy of only 10.7 MeV. Furthermore, most of the remaining strength is spread among seven levels in the giant-resonance region between 10 and 15 MeV. It is not clear whether the improvements needed to move the dipole strength higher in energy (to match the experimentally observed 13.5 MeV) will also tend to concentrate it into a narrower energy region.

There is no significant uncertainty about the excitation energies at which Bi^{208} is left when neutrons are removed from different orbits in Bi^{209}. The energies of these hole states are believed to be almost the same as the energies of the corresponding hole states in Pb^{207} which have been identified experimentally.[24] Calculations[25] using a residual interaction between the neutron hole and proton particle in Bi^{208} indicate that there is but little mixing between configurations and that the splitting of the multiplets is not large. Neutron pickup experiments[26] performed on Bi^{209} tend to support these calculations. The energies of the hole states are given in the first column of Table I.

The wave functions obtained for the dipole state from any of the calculations available for Pb^{208} are obviously incorrect insofar as neutron decay is concerned, because they are only bound state rather than continuum wave functions. In order to estimate direct neutron emission from the dipole state, we used the common approximate procedure which characterizes a single-particle width Γ_{SP} in terms of the penetrability P_l and the reduced width γ^2:

$$\Gamma_{SP}=2P_l\gamma^2. \tag{15a}$$

The reduced width γ^2 is often written as[27]

$$\gamma^2=\theta^2\hbar^2/MR^2, \tag{15b}$$

where M is the nucleon mass and θ is a constant near 1. If $R=1.41A^{1/3}$ F is used, the value of the single-particle width Γ_{SP} for decay to Bi^{208} can be written as

$$\Gamma_{SP}=(1.16\text{ MeV})\theta^2P_l(E_n). \tag{16}$$

The relevant square-well penetrabilities for neutrons are also shown in Table I, for $R=1.41A^{1/3}$ F, and for the hole-state energies appropriate to Bi^{208}. The total resonant direct-emission width of the dipole state Γ_D can be calculated by adding the contributions from the different particle-hole configurations which appear in the dipole state with amplitude α_i; the ith configuration has associated with it a neutron orbital momentum l_i and energy E_{ni}:

$$\Gamma_D=(1.16\theta^2\text{ MeV})\sum_i \alpha_i^2P_{l_i}(E_{ni}). \tag{17}$$

For the wave function shown in Table I and $\theta^2=1$, the width Γ_D in Eq. (17) has the values 0.065, 0.160, and 0.296 MeV at 12, 14, and 16 MeV, respectively. Two refinements would be made in Eq. (17) if one had more confidence in the smaller amplitudes in Table I. Angular factors could be introduced for each of the two-particle states corresponding to one hole state, and the amplitudes would be squared only after they had been added. For the observation angle of 115°, one expects to observe 11.5% more neutrons than average for a p to d transition, and 8.3% more than average for an f to g transition. Thus, the relative correction favoring the d particle emission at 115° is only 2 or 3%, and this refinement is not warranted in the analysis described below. For simplicity, the direct-emission width will be taken as 10% less than that implied by matching experimental data at 115°.

Although the absolute value of the neutron emission width does not enter into fitting the data, it does play an important role in interpreting the fraction of events which are statistical. Within the framework of the usual square-well model for reduced widths, the value of both R and θ^2 can affect the width. Although the reduced width is inversely proportional to R^2, the penetrability is approximately proportional to R, so that the over-all effect on Γ_D of reducing R to $1.2A^{1/3}$ F would be to increase the factor $1.16\theta^2$ to $1.36\theta^2$ without significantly affecting the sum in Eq. (17). On the other hand, values of θ^2 of either 1 or 1.5 have been used. Thus, depending on the choice of θ^2 and of R, the values of Γ_D for 14 MeV according to Table I can vary between 160 and 282 keV.

The oversimplified model which treats the entire giant resonance as though it were a simple resonance[16,18]

[23] E. G. Fuller and E. Hayward, Nucl. Phys. **33**, 431 (1962).
[24] P. Mukherjee and B. L. Cohen, Phys. Rev. **127**, 1284 (1962).
[25] Y. E. Kim and J. O. Rasmussen, Phys. Rev. **135**, B44 (1964).
[26] J. R. Erskine, Phys. Rev. **135**, B110 (1964).
[27] See, for example, A. M. Lane, Rev. Mod. Phys. **32**, 519 (1960). A common variation uses $\theta_1^2=\frac{2}{3}\theta^2$ as in M. H. MacFarlane and J. B. French, *ibid.* **32**, 567 (1960).

implies that the total width of the resonance Γ_t is the sum of the partial widths Γ_D and Γ_C:

$$\Gamma_t \simeq \Gamma_C + \Gamma_D. \tag{18}$$

This also implies that there is no significant direct nucleon emission (from the initial state directly to the final state) except that which is related to the dipole state; insofar as fast photoneutrons are emitted, they arise from the dipole state which acts as an intermediate state. In order to emphasize this important distinction, Wilkinson[16] introduced the term "resonant-direct" to describe these nonstatistical neutrons. In addition, if Γ_C is used to imply eventual emission of a statistical neutron, it is assumed that a negligible number of neutrons are emitted by the more complicated states reached by the system as the dipole state proceeds toward the compound nucleus. This type of emission from the stages of successive complication has recently been invoked to explain nonstatistical nucleons[28] in other nuclear reactions, but it is not clear whether this process would be significant in the giant resonance.

If this simplified model is correct, the observed fraction of statistical processes, $f_S(E_\gamma)$, could be written as

$$f_S = \Gamma_C/\Gamma_t, \tag{19a}$$

$$1 - f_S = \Gamma_D/\Gamma_t. \tag{19b}$$

Equations (19) provides a convenient parametrization of f_S in the analysis which follows, since Eq. (17) can be used to give the energy dependence of Γ_D. The analysis is therefore formulated so that the unknown factor is Γ_C. As suggested by Danos and Greiner[29] we express Γ_C as

$$\Gamma_C(E_\gamma) = \Gamma_{C14}[E_\gamma/(14\ \text{MeV})]^q, \tag{20}$$

where Γ_{C14} is the width for the decay of the dipole state into the compound nucleus at 14-MeV excitation.

IV. RESULTS AND CONCLUSIONS

The 120 data points as presented in Figs. 5 and 6 were always analyzed as a single unit by including both a statistical and a nonstatistical component, as in Eq. (8). To select the best values for the parameters being tested a fitting procedure was used which minimized χ^2 defined as

$$\chi^2 = \sum_k \sum_i \frac{\{[\Delta_i P(U_i, E_{\gamma k})]^{\text{calc}} - [\Delta_i P(U_i, E_{\gamma k})]^{\text{expt}}\}^2}{(\sigma_P)^2}, \tag{21}$$

where σ_P is the error in the experimental value of $\Delta_i P$ inferred from only the statistical error in the number of observed neutrons. Because of this choice of σ_P, the absolute values of χ^2 were not considered significant; relative values were used to select best parameters. The individual fits to the data were examined rather carefully to be sure that the conclusions being reached about some parameters were not at all sensitive to those other parameters which were being held fixed. If any doubts arose, additional calculations were made with different values of the fixed parameters. After some practice, it was relatively easy to draw conclusions about some parameters without allowing all parameters to vary. No attempt will be made to summarize all of the many calculations that were made. The conclusions about the statistical neutrons, the level density in Bi^{209} and the fast-neutron group are given in this section.

A. Confirmation of the Statistical Model

The first analysis was made with only four adjustable parameters: an over-all normalization constant [c of Eq. (3)], one parameter, T or a, to characterize the level density, and two parameters Γ_{C14} and q which describe the energy dependence of Γ_C [Eq. (20)]. No correction was used for effective efficiency. The value of Γ_D was calculated with no adjustable parameters by using Eq. (17), with the single particle-hole amplitudes of Table I, and the square-well penetrabilities appropriate for $R = 1.41A^{1/3}$ F. The kinematic factor $K(E_n)$ was assumed to be E_n.

Quite similar fits were achieved using either constant T [Eq. (10a)] or constant a [Eq. (10b)]; the χ^2 values were 200 and 212, respectively. These fits were particularly informative because they indicated that neither form of the level density adequately described the compound nuclear contributions to low residual energies. Six additional parameters were introduced to characterize the effective level densities $\Delta_i\rho(U_i)$ for $U_i \leq 3.5$ MeV, in order to learn whether the fit could be improved significantly. The calculations with these extra parameters indeed did fit the data considerably better for both forms of the level density (the χ^2 values dropped by about 60 in both cases). The values of $\Delta_i\rho(U_i)$ which fit the data of Fig. 5 are shown by the points in Fig. 7 which also has the curves corresponding to constant T or constant a. Figure 7 makes it clear that neither simple form is adequate for low-excitation energy. When additional calculations were made to test other parameters, $\Delta_i\rho(U_i)$ was left adjustable for $U_i \leq 3.5$ MeV. A constant temperature was used for 4 MeV $\leq U_i \leq$ 6.5 MeV, but over so limited an energy range, either constant T or constant a is adequate. The lines drawn in Fig. 5 correspond to the level density shown in Fig. 7 and a constant nuclear temperature. The apparent temperature is not physically significant except as a lower limit, because the line-shape correction had not been included.

A few calculations were performed to see whether the choice of the particular dipole wave function in Table I was interfering with a better fit. Although

[28] J. J. Griffin, Phys. Rev. Letters **17**, 478 (1966); Phys. Letters **24B**, 5 (1967).
[29] M. Danos and W. Greiner, Phys. Rev. **138**, B876 (1965).

slightly better fits could be obtained by making minor adjustments (χ^2 could be reduced by $\sim 7\%$), it was not clear that these apparent improvements were significant. Because these adjustments did not affect any of the other factors significantly, and because there is a definite advantage to using a wave function derived from a specific calculation, the wave function of Table I was used for all subsequent calculations. In order to allow for the finite resolution, the calculated nonstatistical neutrons were assumed to be distributed with a triangular resolution function 1.5-MeV wide at the base. Other resolution effects were absorbed in the effective efficiency.

The parameters Γ_{C14} and q had only slight effects on the level density parameters and only obvious effects on the fitting of the fast neutrons. (These are discussed in connection with Fig. 10). Because the fraction of events which were statistical, f_S, varied quite slowly with energy, the parameters Γ_{C14} and q were retained as adjustable parameters in all of the calculations.

The experimental data corrected for effective efficiency are shown by the points in Fig. 6. The data in the lowest four 0.5-MeV intervals are combined into 1-MeV intervals because of poor statistics and energy resolution. The energy dependence of the level density corresponding to the best fit is shown in Fig. 8, and the corresponding calculated values are shown by the lines in Fig. 6. Although this fit is not as good as that of Fig. 5, it also strongly supports the statistical model. [The χ^2 for the fit in Fig. 6 is 200, whereas that for Fig. 5 is 140. This difference might be due to systematic errors in the effective efficiency or to the oversimplified choice of $K(E_n)=E_n$. The effect of using a kinematic factor different from E_n will be discussed later.] A very

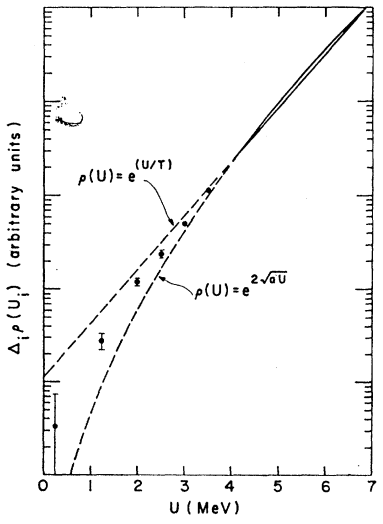

FIG. 7. Apparent level-density parameters for Bi^{208}. The points and solid lines are the result from analysis of the data in Fig. 5. Extrapolations are shown by the dashed lines. The data were not corrected for line shape and are presented to show the effect of that correction which was made for Fig. 8.

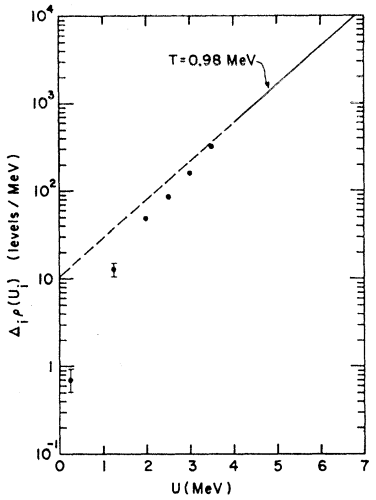

FIG. 8. The level density of Bi^{208}. The points and solid line are the result from analysis of the data in Fig. 6. The vertical scale has been normalized approximately from the known levels (Refs. 25, 26) in Bi^{208}. The fit corresponds to a constant temperature of $T=0.98$ above 4 MeV. The points below 4 MeV would not change significantly if Eq. (10b) were used in place of Eq. (10a).

important feature of both Figs. 5 and 6 is that many experimental points in the upper part of the figures can be fit despite the stringent restrictions of the statistical model. Although these fits are not perfect, they do not show any systematic effects which could be due to a breakdown of the statistical model. They provide a striking confirmation of the model despite the experimental uncertainties associated with the effective efficiency.

B. Experimental Level Density of Bi^{208}

We have enough experimental data to determine the energy dependence of the level density quite independent of any theoretical predictions. About 60 of the data points of Figs. 5 or 6 give information about the relative level densities in the residual excitation-energy range between 3.75 and 6.75 MeV. When this energy region is divided into six intervals of 0.5 MeV, these data strongly overdetermine the five constants which represent the relative level densities in these intervals. The data make it clear that the energy level density increases exponentially in this interval. As is evident in Fig. 7, there is no significant difference between a constant T and a constant a in this energy range. This conclusion is essentially independent of effective efficiency correction.

There are fewer experimental points which give information about the level density below 3.75 MeV where nonstatistical neutrons are important. Nevertheless, there are about 20 data points which can determine the 5 or 6 constants adequately, particularly because the temperature mentioned above determines the effectson the competition due to changes in γ ray energy. Comparison of Figs. 7 and 8 shows that despite

the differences in the nuclear temperature at higher excitations caused by different efficiency corrections, the relative level densities between 1 and 3.5 MeV agree to within the statistical errors.[30] This insensibility of the relative low-lying level densities to the uncertain effective efficiency makes Fig. 8 a reasonable estimate of the level density in the Bi^{208} nucleus. This energy dependence of the level density is consistent with other experiments.[6,15] In Fig. 8 the vertical scale was normalized to give 12 levels/MeV at $U=1.2$ MeV. This approximate normalization was based on the known levels[25,26] in Bi^{208}. A test of this normalization is provided by comparing the level density of Bi^{208} with the observed level density in the similar nucleus Bi^{210}. The level density shown in Fig. 8 for 4.2-MeV excitation is 700 levels/MeV. This implies[31] a level spacing of about 10 keV for levels of 4^- and 5^-, as would be observed when s-wave neutrons interact with Bi^{209}. Experimentally the level spacing when slow neutrons are captured in Bi^{209} is observed to be about 4 keV.[32] In view of the simplicity of the normalization, the uncertainty in the J dependence, and the small amount of neutron-capture data available, the agreement is considered reasonable.

Because of the uncertainty in the effective efficiency, one of the least precise aspects of the level density shown in Fig. 8 is the nuclear temperature above 4 MeV. The value implied by the effective efficiency used to obtain Fig. 8 is 0.98 MeV but it is difficult to find a sound basis for assigning an experimental error. The actual temperature is almost surely higher than 0.8 MeV, and it is quite probably less than 1.15 MeV. The equivalent value of a in Eq. (10b) would be about 5.5/MeV for U near 5.5 MeV.

The level density of Fig. 8 is not consistent with either constant temperature T [Eq. (10a)] or constant a [Eq. (10b)]. It has been suggested[33] that these simple forms be replaced by some form giving an intermediate density, based on a refinement to the Fermi-gas model. The data in Fig. 7 and 8 are indeed intermediate between the constant temperature and constant a. Although there is little justification for considering refinements to the Fermi-gas model in the low-excitation-energy region, especially if there are too few levels to provide a significant statistical sample, we did fit the level density of Fig. 8 above 2 MeV to the form of Eq. (10c) and obtained the values $a'=10.1$/MeV and $\rho_0=2.75\times10^{-2}$/MeV.

In most of our data analysis we used E_n for the kinematic factor $K(E_n)$ introduced in Eq. (9). If angular-momentum effects are neglected, the kinematic factor can be derived with the aid of detailed balance[34]:

$$K(E_n)\propto E_n\sigma_C(E_n)\,, \tag{22}$$

where $\sigma_C(E_n)$ is the cross section for formation of the compound nucleus in the inverse reaction.

Even though our poorly known effective efficiency at low neutron energies makes the question of inverse cross section somewhat academic, we did examine the effect on the analysis of using inverse cross sections calculated with the available optical-model parameters. First the average optical model parameters of Rosen *et al.*[35] were used. The reaction cross section for $A=208$ obtained from this calculation had very little energy dependence (the normalized values changed smoothly from 0.96 at 1 MeV, to 1.0 at 1.6 MeV, 0.95 at 2 MeV, and 0.85 at 4 MeV). When applied to the data of Fig. 5, this cross section had a negligible effect: It raised the temperature by 0.03 MeV and increased χ^2 from 140 to 160. We also tried the optical-model parameters of Auerbach and Moore[36] which had been cited[6] as an important ingredient in the interpretation of the photoneutrons from Bi^{209}. This second calculation yielded a distinctively peaked reaction cross section. The normalized cross section for Bi^{209}, and Pb^{208} in parentheses, are given for comparison with the previous results: 0.63(0.75) at 1 MeV, 0.78(0.88) at 1.4 MeV, 1.0(1.0) at 2.2 MeV, 0.91(0.93) at 3 MeV, and 0.83(0.83) at 4 MeV. When the above inverse cross section for Pb^{208} was used for the data of Fig. 5 (which are uncorrected for line shape), the fit became much worse (χ^2 rose from 140 to 250) as might have been expected. The most important effects and the worst agreement came from the lower-neutron-energy points. This can be understood by considering the two efficiencies shown in Fig. 2. The efficiency uncorrected for late neutron arrivals is surely too low at low energies. The peaked inverse neutron cross section, which multiplies this efficiency curve in the analysis, further lowers the product at low energy. The inferred data points at low energy therefore become hopelessly high. On the other hand, if this peaked inverse cross section were used together with the effective efficiency curve in Fig. 2, at the low energies, it would merely counteract some of the change provided by the effective efficiency. Because the effective efficiency was not known well, the study of the combined effects of the effective efficiency and the peaked inverse cross section was not pursued. Although these calculations showed that our experiment could not decide between the two different inverse cross sec-

[30] The experimental points that determine the level density below 3.5 MeV correspond to neutron energies larger than 3 MeV for which the efficiency is much less uncertain.

[31] This estimate uses a spin cutoff factor of $\sigma=4$ in the usual form of the spin-dependent level-density formula as given for example in Ref. 32.

[32] L. M. Bollinger, in *Nuclear Spectroscopy*, edited by F. Ajzenberg-Selove (Academic Press Inc., New York, 1960), Part A, p. 417.

[33] T. Ericson, Advan. Phys. **9**, 425 (1960); D. Bodansky, Ann. Rev. Nucl. Sci. **12**, 79 (1962).

[34] J. M. Blatt and V. F. Weiskopf, *Theoretical Nuclear Physics* (John Wiley & Sons, New York, 1952).

[35] L. Rosen, J. G. Beery, A. S. Goldhaber, and E. H. Auerbach, Ann. Phys. (N.Y.) **34**, 96 (1965).

[36] E. H. Auerbach and S. O. Moore, Phys. Rev. **135**, B895 (1964).

tions, they did indicate that the conclusions of this paper concerning the fast neutrons are not very sensitive to the shape of the inverse cross section. In particular, despite any uncertainties in the effective level density at low excitation energies, the contribution of statistical neutrons to these residual energies could be inferred by combining the data taken at different γ-ray energies.

C. The Fast-Neutron Group

The inferred separation of the two groups of neutrons (as described in Secs. IV A and IV B) is shown in Fig. 9, in which the circles represent all the neutrons while the crosses represent the nonstatistical excess. The data are the same as shown in Fig. 6 except that they are displayed in 1-MeV intervals. The ordinate is the fraction of neutrons at 115° which correspond to the residual energy intervals shown. To correct for the theoretical angular distribution and obtain the corresponding fractions averaged over all angles, the ordinates, for the nonstatistical neutrons only, should be reduced by about 10%. The proximity of the crosses and the circles in Figs. 9(a) and 9(b) indicates that the nonstatistical neutrons which lead to the lowest 2 MeV in Bi^{208} can be determined relatively well, independent of the uncertainties associated with the statistical neutrons. On the other hand, the nonstatistical neutrons which lead to higher excitation energy are known less accurately for the three following reasons: (1) because of subtraction of two large numbers the absolute uncertainty due to statistical error is greater; (2) the greater number of statistical neutrons (specifically at the lower γ-ray energies) makes the inferred number of nonstatistical neutrons more sensitive to the level-density parameters; (3) the high U, low E_γ combinations correspond to low neutron energies, and hence are subject to the additional uncertainties due to the effective-efficiency correction which was applied to the data to obtain the points in Fig. 9. This uncertainty about the relatively small nonstatistical component leading to higher excitation energy should not obscure the fact that the analysis described above has provided for those neutrons leading to the lowest two MeV in Bi^{208} an essentially unambiguous separation of the statistical from nonstatistical component.

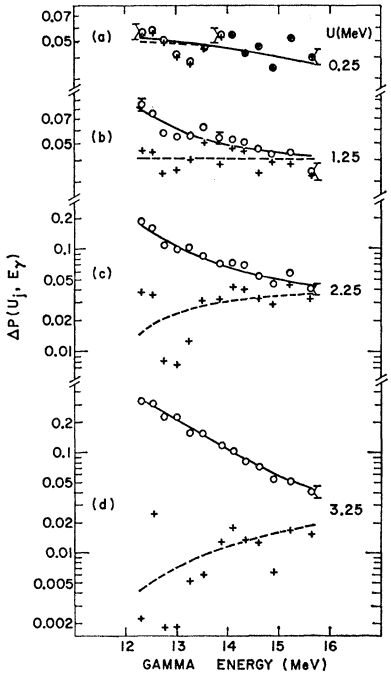

FIG. 9. Probability for photoneutron emission at 115° within the lowest four 1-MeV-wide energy bins. Circles represent all the neutrons while crosses refer to the nonstatistical excess only. The curves are the result of the same least-squares fit of Fig. 6.

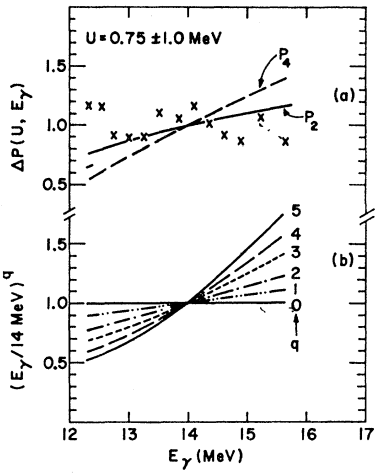

FIG. 10. (a) Normalized fraction of nonstatistical neutrons (×) for the 2-MeV interval centered at 0.75 MeV. (The value 1.0 corresponds to 7.7% if an average over angles is taken.) The lines labeled P_2 and P_4 represent expected energy variations of Γ_D for pure $l=2$ or $l=4$ direct neutron emission, as discussed in the text. The lines show the energy dependence of the neutron penetrability for a square-well potential. (b) Energy variation of Γ_C as predicted by Eq. (20) for different values of q.

The absolute value of the ordinate in Fig. 9 depends on the inferred temperature because this temperature is used to deduce the total number of emitted neutrons. However, the relative ordinates of the different energy groups are insensitive to this number. The curves in Fig. 9, are the result of the same least-squares fit of Fig. 6. The inferred fractions of statistical processes are 0.90, 0.88, and 0.88 at 12.3, 14.1, and 15.6 MeV, respectively. The above numbers were determined within 3.5%.

In order to display the γ-ray energy dependence of the fraction of nonstatistical neutrons, the data for the 2-MeV interval centered at 0.75 MeV excitation in Bi^{208} are shown on a normalized, linear scale in Fig. 10(a). The value 1.0 in this figure would correspond to 8.6% if no correction were made for the angular distribution, or to 7.7% if the correction is made. It is clear from Fig. 10(a) that this group of nonstatistical neutrons is intimately associated with the giant reso-

TABLE II. Relative, resonant-direct neutron-emission probabilities. The relative values are presented as fractions of the total resonant-direct emission at the three γ-ray energies. The expected variation with γ-ray energy of the total resonant-direct neutron emission width is indicated in the bottom row which gives the sums associated with Eq. (17).

Excitation energy of hole state (MeV)	Hole	Particle	Fraction of resonant-direct neutrons which is contributed by each configuration $E_\gamma=12$ MeV	$E_\gamma=14$ MeV	$E_\gamma=16$ MeV
0	$p_{1/2}$	$d_{3/2}$	0.10	0.05	0.03
0.57	$f_{5/2}$	$g_{7/2}$	0.47	0.40	0.31
0.9	$p_{3/2}$	$d_{5/2}$	0.24	0.13	0.09
1.6	$i_{13/2}$	$j_{15/2}$	0.00	0.02	0.08
		$h_{11/2}$	0.01	0.03	0.04
2.3	$f_{7/2}$	$g_{9/2}$	0.14	0.27	0.28
3.5	$h_{9/2}$	$i_{11/2}$	0.00	0.02	0.08
		$g_{7/2}$	0.00	0.03	0.05
	Total		0.96	0.95	0.96
	$\sum_i \mathcal{G}_i^2 P_{li}$		0.055	0.135	0.255

nance. The fraction of photon interactions associated with a nongiant-resonance process would show a substantial dip near 14 MeV, because the total absorption is about twice as big at 14 as it is at 12 or 16 MeV.

The neutron-energy resolution is too poor to permit identification of neutron groups associated with each hole state, but the data tend to support the distribution of residual energies implied by the wave function in Table I. The main nonstatistical strength seems to be associated with one or both of the hole states near 0.75 MeV [i.e., the $(f_{5/2})^{-1}$ or $(p_{3/2})^{-1}$] and with the $(f_{7/2})^{-1}$ hole state near 2.3 MeV. From Fig. 5 and also from the spectra with the best statistics and resolution, it is clear that few neutrons leave Bi^{208} in the $(p_{1/2})^{-1}$ doublet consisting of the ground state and a level at about 60 keV. The $(i_{13/2})^{-1}$ multiplet near 1.6 MeV is also very weakly excited. Direct evidence for this is presented by the dip near 50 nsec in the time-of-flight spectrum of Fig. 3. These experimental conclusions are consistent with the theoretical relative resonant-direct neutron-emission probabilities obtained from Table I and summarized in Table II.

D. The Energy Dependence and Absolute Value of Γ_C

There is no simple consistent interpretation of the energy dependence and the absolute value of Γ_C, the width for the decay of the dipole state into the compound nucleus. If the existence of a single dipole state is assumed, the energy dependence of Γ_C can be inferred directly from the data shown in Fig. 10(a), which should be proportional to $\Gamma_D/(\Gamma_D+\Gamma_C)$. The obvious qualitative feature of the experimental data is that the fractional probability of emitting resonant direct neutrons does not increase significantly with energy despite the marked increase in phase space. Examples of expected energy variations of Γ_D are shown by the two curves in Fig. 10(a) which correspond to normalized square-well penetrabilities (for $R=1.41A^{1/3}$) for the most likely particle angular momenta. The dashed curve corresponds to a particle with $l=4$ while the solid curve is drawn for $l=2$. In this same energy interval, the $l=0$ penetrability, which corresponds to phase space, would have only slightly less energy dependence than is shown for $l=2$; the normalized values for $l=0$ would be 0.80 at 12.3 MeV (instead of 0.75) and 1.10 at 15.7 MeV (instead of 1.15).

The data of Fig. 10(a) make it clear that the fraction of resonant-direct neutrons does not increase as rapidly with energy as would be expected if Γ_C were constant. Independent of the exact details of the wavefunction of the giant-dipole state, the $l=2$ and $l=4$ curves in Fig. 10(a) essentially define the expected γ-ray energy dependence of direct neutron emission from this dipole state to the known hole states in Bi^{208} near 0.75 MeV. (The centrifugal barriers, for $R=1.41A^{1/3}$ F are about 1.9 MeV for $l=2$, 6.3 MeV for $l=4$, 9.5 MeV for $l=5$, and 18 MeV for $l=7$. The dominance of electric dipole absorption therefore implies a p-hole state reached by $l=0$ and $l=2$ neutrons and an f-hole state reached by $l=2$ and $l=4$ neutrons would be more important than the i-hole state which can be reached by $l=5$ and $l=7$ neutrons. These conclusions are indicated quantitatively in Table II.)

The semiquantitative implications of the data in Fig. 10(a) are illustrated in Fig. 10(b), which shows the factor $[E_\gamma/(14\text{ MeV})]^q$ of Eq. (20) for various values of q. If the fraction of nonstatistical neutrons shown in Fig. 10(a) is considered to be constant, independent of γ-ray energy, the curves in Fig. 10(b) [together with Eqs. (19) and (20)] imply that $q=2$ would be required if $l=2$ neutrons dominated while $q=3.5$ would be required if $l=4$ neutrons were most important.

The experimental data related to the hole state near 2.3 MeV, shown in Fig. 9(c), tends to favor the dominance of $l=4$ neutrons and therefore the higher q value. The 1-MeV bin included in Fig. 9(c) is dominated by the $f_{7/2}$ hole; this fact, together with the likely dominance of $l\rightarrow l+1$ transitions,[16,17] implies that $l=4$ neutrons are important. In the energy region above 13.5 MeV in Fig. 9(c), the fraction of nonstatistical neutrons is apparently energy-independent, thus implying a high q value.

These semiquantitative arguments in favor of higher q values were reinforced by the computed fit to the data which minimized χ^2 of Eq. (21). The best fit was obtained for $q=4$, but the large statistical errors associated with the data admitted the entire range $3\leq q\leq 5$ without increasing χ^2 by more than 6%. However, the fits became noticeably worse, particularly for residual energies less than 2.5 MeV, for q values outside this range. The value of $q=4$ corresponds to an increase of Γ_C by a factor of about 3 between 12 and 16 MeV.

A possible flaw in the inferred value of q is implied by the lack of internal consistency between the models

used and the experimental data. The inconsistency becomes apparent if one compares the inferred value of Γ_C with the experimentally observed total width of the giant dipole resonance. The value of Γ_C can be obtained by combining the experimental determination that 12% of the emitted neutrons at 14 MeV are nonstatistical with the calculated value of Γ_D [given by Table II and Eq. (17)]. Depending on the value used for the reduced width [as discussed in the text following Eq. (17)] the inferred value of Γ_C is between 1.2 and 2.1 MeV. Although this range includes values which are less than a factor of 2 below the observed width[15] of 3.8 MeV, there is a definite inconsistency with the simplified development given in Sec. III.

There are at least three different effects which could explain this inconsistency between the observed and inferred total width. First, the maximum value accepted for Γ_D (i.e., the 282 keV mentioned in III B) may be below the correct theoretical value. Second, there might be microscopic fluctuations of Γ_D with energy which could require a correction to the relation between the nonstatistical fraction and the average value of Γ_D given in Eq. (19). (Situations in which branching ratios are not given correctly by average values of partial widths have been discussed in both elastic γ-ray scattering[37] and compound elastic neutron scattering.[38] Either of these two possibilities might remove the width inconsistency without necessarily casting doubt on the existence of a single dipole state or the inferred energy dependence of Γ_C. (Even if this were the case, an additional theoretical treatment would be needed to establish the consistency between the inferred energy dependence of Γ_C and the observed energy dependence of the giant dipole resonance.) A third possible cause of the width inconsistency mentioned above would be the existence of several dipole states within the giant resonance, as implied by the calculations of Gillet *et al.*[22] The existence of several dipole states would invalidate part of the analysis we used [i.e., Eqs. (18)–(19)]. In this case, inferences about Γ_C and Γ_t could not be made without more complete information about the energies of the underlying dipole states, their detailed wave functions, and the way in which they mix.

[37] P. Axel, Phys. Rev. **126**, 671 (1962).
[38] P. Moldauer, Phys. Rev. **123**, 968 (1961).

E. Summary of Conclusions

1. Most of the neutrons emitted after the photoexcitation of Bi^{209} are statistical. The nonstatistical fraction is about 10%, 12%, and 12% at 12, 14, and 16 MeV, respectively. A much more rapid increase in the nonstatistical fraction would be expected due to the increase with energy of both the number of available hole states and the neutron phase space.

2. The energy dependence of the energy-level density was obtained. As shown in Fig. 8, this level density is essentially exponential above 4 MeV (with T about 1 MeV), but there are more levels at low energy than would be implied by an extrapolation of the exponential. Uncertainties about the effective neutron efficiency and the inverse cross section might change the inferred temperature but would not affect the general agreement with the statistical model unless the inverse cross section were perversely pathological.

3. Most, if not all, of the nonstatistical neutrons are intimately connected with the giant resonance. These neutrons are indeed resonant-direct; the dipole state plays the role of a well defined intermediate state insofar as nonstatistical neutron emission is concerned.

4. Unless the intrinsic width for resonant-direct emission decreases rapidly with energy, the data provide a direct experimental indication that the effective partial width Γ_C (for the dissolution of the dipole state into compound nuclear states) increases with energy.

5. The nonstatistical neutrons leave the residual nucleus in the hole states predicted by models which treat the giant resonance as a combination of particle-hole states.

6. The experimental data are consistent with a model in which the entire giant resonance is dominated by a single dipole state, provided that Γ_C increases by a factor of about 3 between 12 and 16 MeV. According to this interpretation, the relative constancy of the fraction of statistical neutrons comes about because both the absolute resonant-direct emission width and Γ_C increase in about the same way. However, this very simple interpretation does not explain either the total width of the giant resonance or its energy dependence. This simple interpretation would imply a total width which is smaller than the observed width by a factor of 1.6 or more.